European Congress on Computational Methods
in Applied Sciences and Engineering (ECCOMAS 2012)
J. Eberhardsteiner et.al. (eds.)
Vienna, Austria, September 10-14, 2012

THERMODYNAMIC MODEL FOR STRAIN-INDUCED CRYSTALLIZATION IN RUBBER

L. Thien-Nga[1], J. Guilie[2], and P. Le Tallec[1]

[1]LMS
Ecole Polytechnique 91128 Palaiseau FRANCE
e-mail: tnle@lms.polytechnique.fr

[2]LMS-Michelin
Ecole Polytechnique 91128 Palaiseau FRANCE
e-mail: joachim.guilie@gmail.com

[1]LMS
Ecole Polytechnique 91128 Palaiseau FRANCE
e-mail: patrick.letallec@polytechnique.edu

Keywords: strain-induced crystallization, rubber, thermodynamic, phase change

Abstract. *Natural rubber (NR) is known to crystallize under strain (SIC) so that NR samples subjected to loading-unloading cycles exhibit hysteresis. A brief review of the numerous experiments conducted on this material is given. Detailed information on the microstructure is therefore available, particularly simultaneous measurements of stress versus elongation and crystallinity versus elongation. Introducing an internal variable associated to crystallinity, a solution to the evolution of this variable can be found, that is thermodynamically consistent. This variable enable us to obtain good laws for both stress-strain and crystallinity-strain curves. This model is assessed by uniaxial tensil tests under cyclic loadings.*

1 Introduction

Natural rubber (NR) exhibits interesting properties due to strain-induced crystallization (SIC) : for instance, fatigue lifetime is known to be modified by this microstructural evolution [8]. In this material, alignment of the polymer chains due to strain modifies the melting temperature of the material, thus creating strain-induced crystallization. There is also accumulation of crystallites during cyclic loading, which again modifies mechanical cycling experiments. The complexity of these thermomechanical phenomena has made understanding and modelling of the mechanical behaviour difficult. Nevertheless, thanks to the important experimental work that has been published up to now, it has become easier to determine what criteria a good model should obey [2, 6].

The main problem stems from the fact that the constitutive aspects under stress have not yet been set, and that some of the constitutive mechanisms identified so far contradict each other [9, 7]. We therefore first review in section 2 state-of-the-art experiments, insisting on what we think are the constitutive aspects of cyclic behaviour. We then construct in section 3 an adequate free energy and chose the internal variables. Thermodynamical consistency is formulated then, and yields constitutive equations for stress, entropy, and the thermodynamical force for crystallization. This enables us to develop evolution laws to be plugged into numerical models. The model is then verified by numerical testing in section 4 and 5.

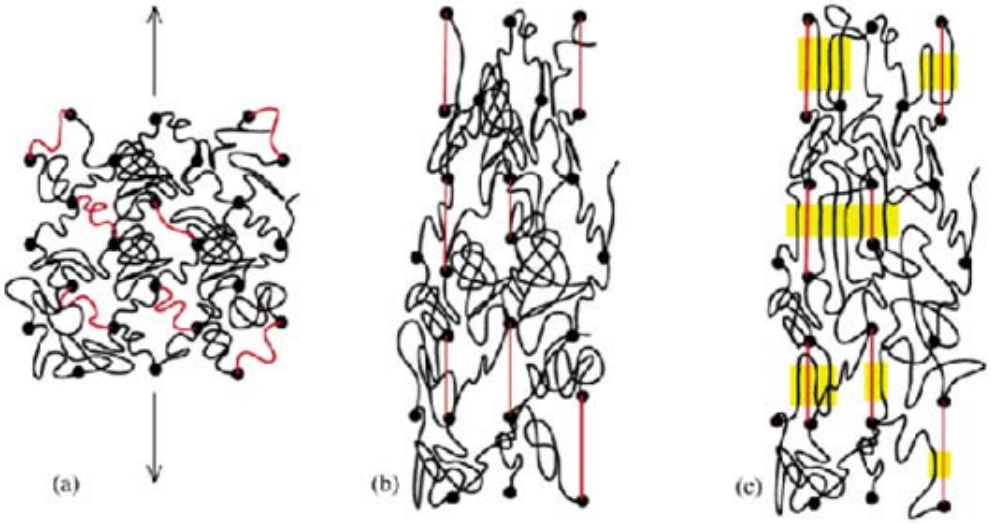

Figure 1: Strain-induced crystallization in NR - Scheme

2 Experimental mechanical behaviour of NR in relationship with microstructure [2]

Because it yields numerous material structure properties, Wide Angle X-ray Diffraction (WAXD) [10] has been the main tool used, among the numerous existing techniques, in order to characterize SIC in rubber. We therefore refer to these WAXD studies to describe the evolution of the semi-crystalline phase of NR encountered when at ordinary conditions of stress and temperature.

2.1 Characterization of the crystalline phase of NR

We are interested in the fine characterization of the semi-cristalline rubber material, particularly the cristallized part, at a nanometer scale. Typical crystallites have dimensions of the order of 10 nm. The crystalline phase can be identified by X-ray diffraction. Random orientation of the crystallites yield circles. If preferred orientation exist these typical diffraction circles are transformed into a structure of spots. The usual spot pattern displays (200), (120) and (002) as the most intense spots. The structured pattern of diffraction gives quantitative structural elements such as lattice parameters. The structure of bulk crystalline material can be obtained by analyzing the distances between spots in the diffraction pattern, each spot being associated to a particular set of crystal planes. It has been found orthorhombic with a=12.3 A, b=8.3 A, c=8.1 A, or sometimes monoclinic but with a structure very close to the orthorhombic's parameters. The main point to remember is that the cell has 4 parallel chains. There are both covalent and Van der Waals interactions within the unit cell. Under uniaxial extension, the interplanar distances are modified up to few percents of the standard distances : a and b are diminished while c increases. Additional information can be extracted from these patterns :

- Sample cristallinity can be deduced by measuring the diffuse halo's intensity, which stems from the amorphous phase only
- The distribution around the average angle associated to elongated streaks can also be observed.
- The broadening of diffraction peaks is detected.

To complete the preceding information about crystallites, the morphology of these crystallites must be observed. The general opinion regarding morphology [2] is that we have no lamellar growth at high elongations but that there may be fibrillar and lamellar structures at intermediate elongation.

2.2 Cyclic mechanical behaviour

There are different ways of performing mechanical experiments on strain-crystallizing rubber. For example, relaxation tests bring information on the characteristics of the phase change[11]. Nevertheless we chose to study mainly cyclic testing, under uniaxial extension, at constant temperature and speed [3]. Sample cristallinity is measured continuously, in real time by using a synchrotron [2]. Part of the experiment is an out-of equilibrium measurement even if speed is very low. It is to be noted that several cycles must be performed prior to real testing, in order to avoid interpretations errors due to the Mullins effect [1].

During uniaxial tension experiments, crystallization appears in natural rubber if amplitude of loading is sufficient. When a loading cycle is applied at ambient temperature, the strain is not the same during loading as on unloading. There is hysteresis. The loading cycle can be "seen" either on the stress-elongation curve, or on the crystallinity curve. One observes generally crystallization, when the sample is loaded; fusion, when the sample is unloaded. One can sometimes observe crystallization at the beginning of the unloading phase. At a given temperature, fusion and crystallization do not happen for the same value of elongation. This is best seen in figure 2.

Several characteristic points appear in the loading cycle, that can be used as benchmarks. These special points are noted O, A, B in the elongation phase, C, D, E in the unloading phase. In order to interpret the results it is useful to list the phenomena at play : crystallization and

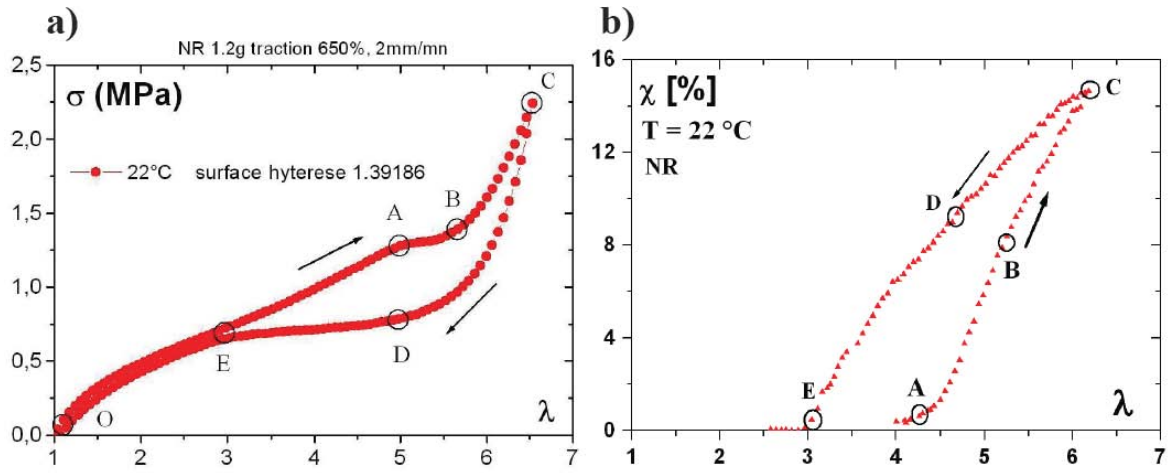

Figure 2: Evolution of a) stress σ and b) crystallinity over a cycle with a speed of $2\,mm/min$ (taken from [3])

melting, hysteresis, relaxation of the amorphous phase, hardening of the polymeric network, supercooling.

Crystallization increases with strain, as shown in the figure 2. After a nearly linear increase, λ reaches a maximum, at point C . It then decreases in the same way, meaning that melting of the crystallites has happened, until complete recovery. Hysteresis is seen : the strain trajectory is not a reversible one. It may be caused as a consequence of several effects: viscoelasticity (associated with disentanglement of the polymer's chains), damage (Mullins effect), or crystallinity. The latter is the best candidate to explain the majority of the hysteresis [3]. Relaxation of the amorphous phase is happening in A-C figure 2. At the end of crystallization the slope of the stress curve is noticeably higher than the simulated curve for a totally amorphous phase [3]. This proves that the material hardens when crystallization occurs. Finally the melting temperature is seen to shift with stress (figure 3), so that crystallites exist above the standard melting temperature at strain equal to zero. This shift is parallel to the crystallization temperature shift in a way that crystallinity is always higher in melting than in crystallization.

The path in the stress-strain curve is now divided in steps going through points A,B,C,D,E :

- From O to A, $1 < \lambda < \lambda_A$, there are no traces of cristallinity in the sample, until $\lambda_A = 4$. The sample is totally amorphous.

- From A to B, $\lambda_A < \lambda < \lambda_B$, crystallinity increases linearly with elongation λ. The stress plateau which occurs can be seen to derive from two opposing mechanisms. On one hand, the crystallization allows the amorphous par of the chains to relax, causing the stress to decrease. On the other hand, the system gets harder. Indeed, the number of crystallites increases, and, when multichain crystallites come into play, these may act as network junctions, increasing functionality thereby.

- From B to C, $\lambda_B < \lambda < \lambda_C (\sim 7)$, B is an inflection point on the cristallinity curve. At that point cristallization starts to slow down and hardening is taking the lead.The mechanism which comes into play could be a change in the morphology of crystallites or percolation. They will form cages that inhibit relaxation of the amorphous chains more easily. The network density will be higher. All these elements can also contribute to slowing down of the relaxation.

- From C to E, $\lambda_C < \lambda < \lambda_E (\sim 3)$, we are in fusion. The mechanisms at play are the same as from A to C, but with a higher cristallinity, due to supercooling: crystallites that would normally have melted at a given temperature without strain are still there due to the presence of strain.

We can associate to this interpretation the dependence of σ_A and σ_E on temperature which emphasize on the supercooling effect (figure 3).

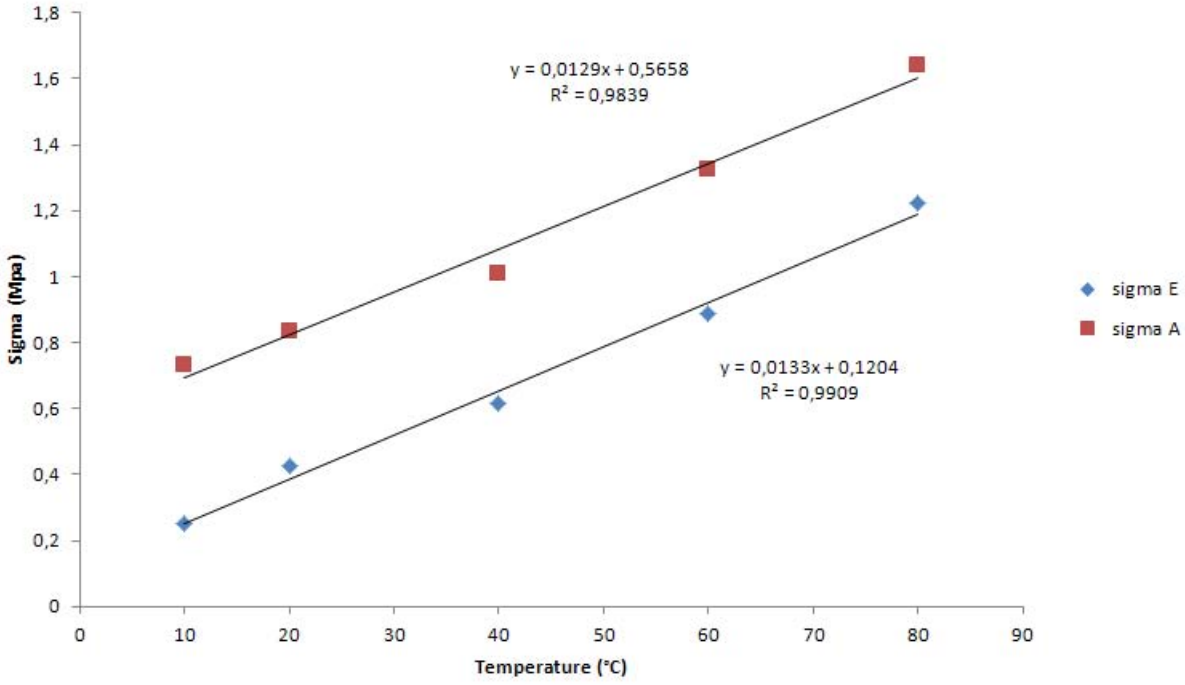

Figure 3: Supercooling effect constructed from data in [3]

3 Constitutive 1D model of strain-induced crystallizing rubber

3.1 Free energy and internal variables

The above interpretation of experimental data is now used to construct a 1D constitutive law which must be in agreement with the second law of thermodynamics. A constitutive law for the amorphous part must first be constructed to model the mechanical beahvior of the rubber in the absence of crystallization.We use the Miehe's model [5], where a polymer chain is constrained inside a tube. In view of on-going work, this model can also be integrated in a directional 3D approach [4]. In that model the chain is assumed to follow the behaviour of a Langevin spring, in interaction with the network.The behaviour is thus determined by chain elongation, tube contraction and temperature.

In more details, we introduce a representative chain whose elementary response is supposed to represent the average response of the material. The chain is assumed to be made of N_{seg} each of length l_{seg} so the total length is $L = N_{seg} l_{seg}.$. The average length of the chain at rest is $r_0 = l_{seg}\sqrt{N_{seg}}$. The elongation λ is defined as ratio of the end-to-end distance to the initial length r_0, and is assumed to be governed by the macroscopic elongation in the considered

direction

$$\lambda = \frac{r}{r_0}. \tag{1}$$

In addition we take into account finite extensibility of the chain, by modeling the free energy of our representative chain by the Langevin potential

$$\psi_f = k_B T N_{seg} \left[\frac{\lambda}{\sqrt{N_{seg}}} L^{-1}\left(\frac{\lambda}{\sqrt{N_{seg}}}\right) + \ln \frac{L^{-1}\left(\frac{\lambda}{\sqrt{N_{seg}}}\right)}{\sinh\left(L^{-1}\left(\frac{\lambda}{\sqrt{N_{seg}}}\right)\right)} \right], \tag{2}$$

with L^{-1} is the inverse Langevin function. The tube contraction energy accounts for repulsion between different chains. The chain is confined to a tube of diameter d which stores a free energy of the form

$$\psi_c = k_B T N_{seg} \left[\alpha \left(\frac{l_{seg}}{d_0}\right)^2 ln(\lambda) \right], \tag{3}$$

which blows up when $\lambda \to 0$. It is then assumed that the two energies can simply be added so that, for n_{ch} chains, we will have from 2 and 3.

$$\psi_{am}(\lambda, T) = n_{ch} k_B N_{seg} T \left[F_\beta \left(\frac{\lambda}{\sqrt{N_{seg}}}\right) + U ln(\lambda) \right], \tag{4}$$

with

- $F_\beta\left(\frac{\lambda}{\sqrt{N_{seg}}}\right) = \frac{\lambda}{\sqrt{N_{seg}}} L^{-1}\left(\frac{\lambda}{\sqrt{N_{seg}}}\right) + \ln \frac{L^{-1}\left(\frac{\lambda}{\sqrt{N_{seg}}}\right)}{\sinh\left(L^{-1}\left(\frac{\lambda}{\sqrt{N_{seg}}}\right)\right)}$ the Langevin energy,
- $U = \alpha\left(\frac{l_{seg}}{d_0}\right)^2$ the tube modulus.

We can now construct a model for the semi-crystalline system. Three additional constitutive mechanisms are introduced :

- relaxation within the amorphous phase,
- network hardening due to morphology change or percolation of crystallites,
- crystal-based increased elasticity observed at high elongation.

Relaxation is taken into account by introducing an internal variable λ_χ to measure the inelastic part of elongation induced by crystallization transforming the free energy into

$$\psi_{sc}(\lambda, \lambda_\chi, T) = n_{ch} k_B N_{seg} T \left[F_\beta \left(\frac{\lambda - \lambda_\chi}{\sqrt{N_{seg}}}\right) + U ln(\lambda) \right]. \tag{5}$$

The effect of hardening by the crystallites is still unclear. Therefore the interaction between the amorphous and crystalline parts is modelled phenomenologically by a function $g(\lambda_\chi, \lambda_{\chi,sat})$ (see figure 4) meant to be the energy stored during phase transformation. By chosing this shape of g, we express the fact that there is saturation for $\lambda_\chi = \lambda_{\chi,sat}$ by making the stored enegy go to infinity for $\lambda_\chi > \lambda_{\chi,sat}$.

The part dealing with crystal effects is then complete if we add to these terms :

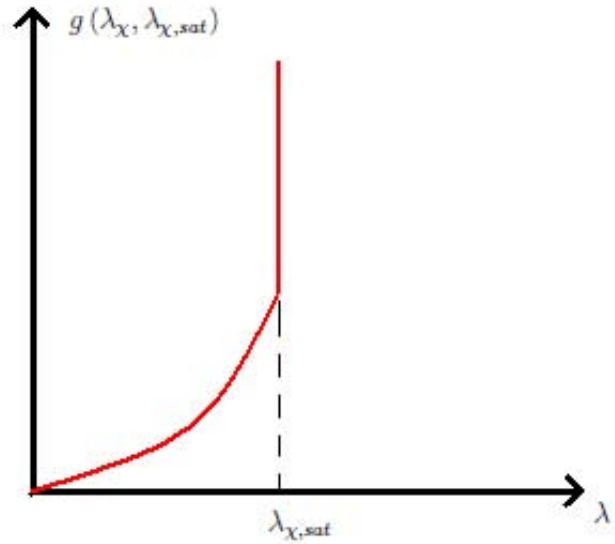

Figure 4: Stored energy

- a free energy introducing to elastic stiffening at high elongations $\psi_{el}(\lambda) = F\left(\langle\lambda - \lambda^*\rangle_+\right)$, where F is a power function, and $\langle\lambda - \lambda^*\rangle_+ = \frac{|\lambda-\lambda^*|+(\lambda-\lambda^*)}{2}$,
- a term corresponding to temperature effect (latent heat is produced or absorbed on crystallization or fusion) $\psi_T = n_{ch}\lambda_\chi(s_f T - h_f)$ where s_f and h_f are respectively the entropy and enthalpy of formation for the crystallite.

Altogether we propose the following free energy for a partially crystallized rubber

$$\begin{aligned}\psi_{sc}(\lambda, \lambda_\chi, T) = \; & n_{ch}k_B R_A T\left[F_\beta\left(\frac{\lambda-\lambda_\chi}{\sqrt{N_{seg}}}\right) + Uln(\lambda)\right] + n_{ch}g(\lambda_\chi, \lambda_{\chi,sat}) \;, \\ & + n_{ch}\lambda_\chi(s_f T - h_f) + n_{ch}k_B R_B T F\left(\langle\lambda - \lambda^*\rangle_+\right)\end{aligned} \tag{6}$$

with R_A and R_B two phenomenological constants.

3.2 Constitutive equations

Constitutive equations are given by imposing that dissipation per unit volume in reference configuration is positive in any process and is supposed to cancel for an elastic or quasistatic evolution

$$D = P\frac{\mathrm{d}\lambda}{\mathrm{d}t} - \frac{\mathrm{d}\psi_{sc}}{\mathrm{d}t} - s\frac{\mathrm{d}T}{\mathrm{d}t} \geq 0. \tag{7}$$

with P the stress in 1D model and s the entropy. By construction ψ_{sc} can be developed into

$$\frac{\mathrm{d}\psi_{sc}(\lambda, \lambda_\chi, T)}{\mathrm{d}t} = \frac{\partial\psi_{sc}}{\partial\lambda}\frac{\mathrm{d}\lambda}{\mathrm{d}t} + \frac{\partial\psi_{sc}}{\partial\lambda_\chi}\frac{\mathrm{d}\lambda_\chi}{\mathrm{d}t} + \frac{\partial\psi_{sc}}{\partial T}\frac{\mathrm{d}T}{\mathrm{d}t}. \tag{8}$$

The absence of dissipation in an isothermal evolution with constant cristallinity yields

$$P = \frac{\partial\psi_{sc}}{\partial\lambda} = P_{am} + P_{tube} + P_{el}, \tag{9}$$

where

- $P_{am} = n_{ch} R_A T L^{-1} \left(\frac{\lambda - \lambda_\chi}{\sqrt{N_{seg}}} \right)$,
- $P_{tube} = n_{ch} R_A T U \lambda^{-1}$,
- $P_{el} = n_{ch} R_B T \frac{\langle \lambda - \lambda^* \rangle_+}{|\lambda - \lambda^*|} \frac{\partial F\left(\langle \lambda - \lambda^* \rangle_+\right)}{\partial \lambda}$.

The absence of dissipation in a quasistatic process yields the entropy law

$$s = -\frac{\partial \psi_{sc}}{\partial T} = \begin{array}{l} -n_{ch} R_A F_\beta \left(\frac{\lambda - \lambda_\chi}{\sqrt{N_{seg}}} \right) - n_{ch} R_A U ln(\lambda) - n_{ch} R_B F \left(\langle \lambda - \lambda^* \rangle_+ \right) \\ -n_{ch} \lambda_\chi s_f. \end{array} \tag{10}$$

Introducing the dual variable associated to $\lambda_\chi$as the thermodynamical force

$$\pi = -\frac{\partial \psi_{semi-cris}}{\partial \lambda_\chi} = P_{am} - n_{ch} \frac{\mathrm{d}g\left(\lambda_\chi, \lambda_{\chi,sat}\right)}{\mathrm{d}\lambda_\chi} - n_{ch}\left(s_f T - h_f\right), \tag{11}$$

and taking into account 9 and 10, the dissipation is finally reduced to:

$$D = \pi \frac{\mathrm{d}\lambda_\chi}{\mathrm{d}t} \geq 0. \tag{12}$$

We now need to introduce and identify a constitutive equation governing the evolution of λ_χ, which must be such that 12 is systematically specified in any possible evolution of the system. It should be noted here that π_{λ_χ} is specified by 11 as a function of the thermodynamical variables λ,λ_χ, T and that it may a priori take positive as well as negative values.

3.3 Evolution laws

We will assume that fusion occurs in equilibrium ($\pi = 0$ if $\frac{d\lambda_\chi}{dt} < 0$) and we know from 12 that π must be positive in crystallization ($\frac{d\lambda_\chi}{dt} > 0$). We define the evolutions law by comparison to the equilibrium

$$\pi\left(\lambda_{\chi,eq}, \lambda, T\right) = 0. \tag{13}$$

We will suppose that crystallization can only occur for sufficiently large thermodynamical forces. Hence, we introduce as in plasticity a yield limit for the thermodynamical force π characterised by

$$Y = Y_1\left(\lambda_{\chi,sat} - \lambda_\chi\right), \tag{14}$$

Above, Y_1 is assumed to be a material constant. The dependence of the yield limit with $(\lambda_{\chi,sat} - \lambda_\chi)$ expresses that the difference between crystallization and fusion curves should decrease to zero when reaching the saturation limit $\lambda_{\chi,sat}$ of crystallization. Figure 5 captions different cyclic paths of crystallization. In our model, crystallization and fusion curves coincide at $\lambda_\chi = \lambda_{\chi,sat}$. And when elongation stops before saturation, there is a plateau between the two curves linearly decreasing with the distance to saturation. In addition, we will impose that the constant Y_1 is such that $n_{ch} \frac{\mathrm{d}^2 g(\lambda_\chi, \lambda_{\chi,sat})}{\mathrm{d}\lambda_\chi^2} > Y_1$ which guarantees that we have

$$\frac{\partial \pi}{\partial \lambda_\chi} = \frac{\partial P_{am}}{\partial \lambda_\chi} - n_{ch} \frac{\mathrm{d}^2 g\left(\lambda_\chi, \lambda_{\chi,sat}\right)}{\mathrm{d}\lambda_\chi^2} \leq -n_{ch} \frac{\mathrm{d}^2 g\left(\lambda_\chi, \lambda_{\chi,sat}\right)}{\mathrm{d}\lambda_\chi^2} \leq -Y_1. \tag{15}$$

So, the different evolutions cases are defined by :

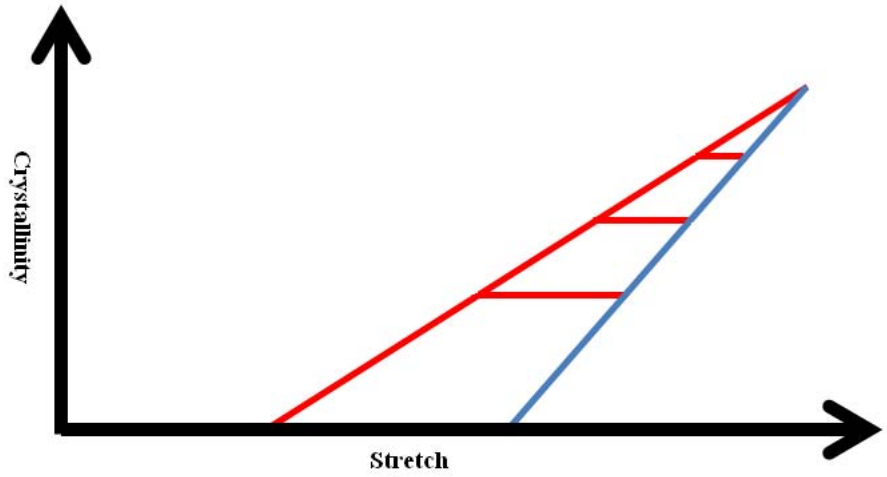

Figure 5: Evolution scheme of crystallinity versus stretch, (Loading in blue) (Unloading in red)

1. If $0 < \pi < Y_1(\lambda_{\chi,sat} - \lambda_\chi)$ then $\frac{\mathrm{d}\lambda_\chi}{\mathrm{d}t} = 0$ so that $D = 0$: the regime is elastic.

2. If $\pi = 0$ and $\frac{\partial \pi}{\partial \lambda}\frac{\mathrm{d}\lambda}{\mathrm{d}t} + \frac{\partial \pi}{\partial T}\frac{\mathrm{d}T}{\mathrm{d}t} \geq 0$, we take $\frac{\mathrm{d}\lambda_\chi}{\mathrm{d}t} = 0$ hence $D = 0$. The regime is also elastic.

3. If $\pi = 0$ and $\frac{\partial \pi}{\partial \lambda}\frac{\mathrm{d}\lambda}{\mathrm{d}t} + \frac{\partial \pi}{\partial T}\frac{\mathrm{d}T}{\mathrm{d}t} < 0$, we take $\frac{\mathrm{d}\lambda_\chi}{\mathrm{d}t} = \frac{\frac{\partial \pi}{\partial \lambda}\frac{\mathrm{d}\lambda}{\mathrm{d}t} + \frac{\partial \pi}{\partial T}\frac{\mathrm{d}T}{\mathrm{d}t}}{-\frac{\partial \pi}{\partial \lambda_\chi}}$. From 15 $\frac{\mathrm{d}\lambda_\chi}{\mathrm{d}t} < 0$. This part represents fusion. We have here $\pi = 0$ and $\frac{\mathrm{d}\pi}{\mathrm{d}t} = 0$, hence $D = 0$.

4. If $\pi = Y_1(\lambda_{\chi,sat} - \lambda_\chi) \geq 0$ and $\frac{\partial \pi}{\partial \lambda}\frac{\mathrm{d}\lambda}{\mathrm{d}t} + \frac{\partial \pi}{\partial T}\frac{\mathrm{d}T}{\mathrm{d}t} \leq 0$, we take $\frac{\mathrm{d}\lambda_\chi}{\mathrm{d}t} = 0$, hence $D = 0$. The regime is again elastic.

5. If $\pi = Y_1(\lambda_{\chi,sat} - \lambda_\chi) > 0$ and $\frac{\partial \pi}{\partial \lambda}\frac{\mathrm{d}\lambda}{\mathrm{d}t} + \frac{\partial \pi}{\partial T}\frac{\mathrm{d}T}{\mathrm{d}t} > 0$, we take $\frac{\mathrm{d}\lambda_\chi}{\mathrm{d}t} = \frac{\frac{\partial \pi}{\partial \lambda}\frac{\mathrm{d}\lambda}{\mathrm{d}t} + \frac{\partial \pi}{\partial T}\frac{\mathrm{d}T}{\mathrm{d}t}}{-\frac{\partial \pi}{\partial \lambda_\chi} - Y_1}$. From 15, we have $\frac{\mathrm{d}\lambda_\chi}{\mathrm{d}t} > 0$. This is a crystallization with dissipation $D = Y_1\left(\lambda_{\chi,sat} - \lambda_\chi\right)\frac{\mathrm{d}\lambda_\chi}{\mathrm{d}t} > 0$.

Finally we cannot have $\pi = Y_1(\lambda_{\chi,sat} - \lambda_\chi) \leq 0$, because the free energy has been constructed so that $\lambda_\chi \leq \lambda_{\chi,sat}$.

To understand the evolution laws, we sum up the different cases on the figure 6.

4 Numerical testing: semi-analytic case

We use a simplified model that will help us understand how this model works and reproduces the essential features of the stress-strain curves. The model parameters are obtained by using the phase diagram. Moreover, we assume that the loading stops at $\lambda_\chi = \lambda_{\chi,sat}$. Finally, we compute the material's response to a loading cycle with imposed elongation and compare its main features to the experimental curves.

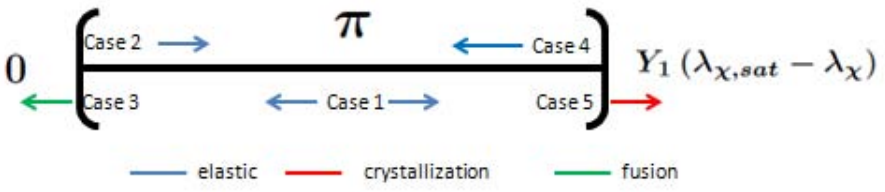

Figure 6: Scheme of the different evolution cases

4.1 Free energy and dissipation potential

In order to simplify the expression of free energy, we take a single chain ($n_{ch} = 1$) and we suppress the repulsion term ($U = 0$). The functions F_β and F are replaced by linear springs

$$R_A T F_\beta\left(\frac{\lambda-\lambda_\chi}{\sqrt{N_{seg}}}\right) \simeq R_{A-G}T\frac{(\lambda-\lambda_\chi)^2}{2}, \tag{16}$$

$$F = \frac{\langle\lambda-\lambda_*\rangle_+^2}{2}. \tag{17}$$

Stored energy is assumed to take the parabolic form

$$g(\lambda_\chi,\lambda_{\chi,sat}) = \left\{\begin{array}{l} g_1\frac{\lambda_\chi^2}{2} \text{ si } \lambda_\chi \le \lambda_{\chi,sat} \\ \infty \text{ si } \lambda_\chi > \lambda_{\chi,sat}\end{array}\right. , \tag{18}$$

With this choices, the free energy reduces to

$$\begin{array}{rl}\psi_{sc}(\lambda,\lambda_\chi,T) = & R_{A-G}T\frac{(\lambda-\lambda_\chi)^2}{2} + g(\lambda_\chi,\lambda_{\chi,sat}) + R_BT\frac{\langle\lambda-\lambda_*\rangle_+^2}{2} \\ & +\lambda_\chi(s_fT-h_f),\end{array} \tag{19}$$

We therefore have the constitutive law

$$P(\lambda,\lambda_\chi,T) = \left\{\begin{array}{l} R_{A-G}T(\lambda-\lambda_\chi) \text{ if } \lambda<\lambda_* \\ R_{A-G}T(\lambda-\lambda_\chi) + R_BT(\lambda-\lambda_*). \text{ if } \lambda\ge\lambda_*.\end{array}\right. \tag{20}$$

Introducing $P_1(\lambda,\lambda_\chi,T) = R_{A-G}T(\lambda-\lambda_\chi)$, the thermodynamical force π is reduced to

$$\pi = P_1(\lambda,\lambda_\chi,T) - s_fT + h_f - g_1\lambda_\chi. \tag{21}$$

4.2 Cyclic stress-strain curves

The beginning of the cycle displays a linear dependence of stress on elongation. The stiffness coefficient R_{A-G} can easily be extracted. Three additional conditions at special points A, C, E can be used. At the start of crystallization (point A) and at the end of fusion (point E) we know that $\lambda_\chi = 0$.

$$P_1(\lambda_A,0,T) - s_fT + h_f = Y_1\lambda_{\chi,sat}. \tag{22}$$

$$P_1(\lambda_E,0,T) - s_fT + h_f = 0. \tag{23}$$

When $\lambda_\chi = \lambda_{\chi,sat}$ the stress σ_C is the same during fusion than during crystallization by hypothesis of saturation

$$P_1\left(\lambda_C, \lambda_{\chi,sat}, T\right) - s_f T + h_f - g_1 \lambda_{\chi,sat} = 0. \tag{24}$$

The linear dependence of $P_1\left(\lambda_A, 0, T\right)$ and $P_1\left(\lambda_E, 0, T\right)$ on temperature agrees with the phase diagram (figure 3). We therefore assume that $P_1\left(\lambda_E, 0, T\right)$ can be written as

$$P_1\left(\lambda_E, 0, T\right) = C_{fus} T + P_1\left(\lambda_E, 0, T_E\right). \tag{25}$$

From the relations 22 to 25, we get

$$h_f = P_1\left(\lambda_E, 0, T_E\right), \tag{26}$$

$$s_f = C_{fus}, \tag{27}$$

$$Y_1 = \frac{P_1\left(\lambda_A, 0, T\right) - P_1\left(\lambda_E, 0, T\right)}{\lambda_{\chi,sat}}, \tag{28}$$

$$g_1 = \frac{P_1\left(\lambda_C, \lambda_{\chi,sat}, T\right) - P_1\left(\lambda_E, 0, T\right)}{\lambda_{\chi,sat}}. \tag{29}$$

With these constants, during fusion, we have

$$P_1\left(\lambda, \lambda_\chi, T\right) - P_1\left(\lambda_E, 0, T\right) - \left(P_1\left(\lambda_C, \lambda_{\chi,sat}, T\right) - P_1\left(\lambda_E, 0, T\right)\right) \frac{\lambda_\chi}{\lambda_{\chi,sat}} = 0, \tag{30}$$

and during crystallization

$$P_1\left(\lambda, \lambda_\chi, T\right) - P_1\left(\lambda_A, 0, T\right) - \left(P_1\left(\lambda_C, \lambda_{\chi,sat}, T\right) - P_1\left(\lambda_A, 0, T\right)\right) \frac{\lambda_\chi}{\lambda_{\chi,sat}} = 0. \tag{31}$$

By using the expression of P_1we then derive the evolution of λ_χ in fusion

$$\lambda_\chi = \frac{R_{A-G} T \lambda}{R_{A-G} T + \frac{P_1(\lambda_C, \lambda_{\chi,sat}, T) - P_1(\lambda_E, 0, T)}{\lambda_{\chi,sat}}} - \frac{P_1\left(\lambda_E, 0, T\right)}{R_{A-G} T + \frac{P_1(\lambda_C, \lambda_{\chi,sat}, T) - P_1(\lambda_E, 0, T)}{\lambda_{\chi,sat}}}, \tag{32}$$

and in crystallization

$$\lambda_\chi = \frac{R_{A-G} T \lambda}{R_{A-G} T + \frac{P_1(\lambda_C, \lambda_{\chi,sat}, T) - P_1(\lambda_A, 0, T)}{\lambda_{\chi,sat}}} - \frac{P_1\left(\lambda_A, 0, T\right)}{R_{A-G} T + \frac{P_1(\lambda_C, \lambda_{\chi,sat}, T) - P_1(\lambda_A, 0, T)}{\lambda_{\chi,sat}}}. \tag{33}$$

The slope of these curves is shown to be larger during crystallization than during fusion because

$$P_1\left(\lambda_C, \lambda_{\chi,sat}, T\right) - P_1\left(\lambda_A, 0, T\right) < P_1\left(\lambda_C, \lambda_{\chi,sat}, T\right) - P_1\left(\lambda_E, 0, T\right), \tag{34}$$

which is observed in the experimental crystallinity curves. Similarly, we have for the stress curve in fusion

$$P = \begin{cases} R_{A-G} T \left(1 - \frac{1}{1 + \frac{P_1(\lambda_C, \lambda_{\chi,sat}, T) - P_1(\lambda_E, 0, T)}{R_{A-G} T \lambda_{\chi,sat}}}\right) \lambda + \frac{P_1(\lambda_E, 0, T)}{1 + \frac{P_1(\lambda_C, \lambda_{\chi,sat}, T) - P_1(\lambda_E, 0, T)}{R_{A-G} T \lambda_{\chi,sat}}} & \text{if } \lambda < \lambda_* \\ R_{A-G} T \left(1 - \frac{1}{1 + \frac{P_1(\lambda_C, \lambda_{\chi,sat}, T) - P_1(\lambda_E, 0, T)}{R_{A-G} T \lambda_{\chi,sat}}}\right) \lambda + \frac{P_1(\lambda_E, 0, T)}{1 + \frac{P_1(\lambda_C, \lambda_{\chi,sat}, T) - P_1(\lambda_E, 0, T)}{R_{A-G} T \lambda_{\chi,sat}}} + R_B T \left(\lambda - \lambda_*\right). & \text{if } \lambda \geq \lambda_*, \end{cases} \tag{35}$$

and in crystallization

$$P = \begin{cases} R_{A-G}T\left(1 - \frac{1}{1+\frac{P_1(\lambda_C,\lambda_{\chi,sat},T)-P_1(\lambda_A,0,T)}{R_{A-G}T\lambda_{\chi,sat}}}\right)\lambda + \frac{P_1(\lambda_A,0,T)}{1+\frac{P_1(\lambda_C,\lambda_{\chi,sat},T)-P_1(\lambda_A,0,T)}{R_{A-G}T\lambda_{\chi,sat}}} & \text{si } \lambda < \lambda_* \\ R_{A-G}T\left(1 - \frac{1}{1+\frac{P_1(\lambda_C,\lambda_{\chi,sat},T)-P_1(\lambda_A,0,T)}{R_{A-G}T\lambda_{\chi,sat}}}\right)\lambda + \frac{P_1(\lambda_A,0,T)}{1+\frac{P_1(\lambda_C,\lambda_{\chi,sat},T)-P_1(\lambda_A,0,T)}{R_{A-G}T\lambda_{\chi,sat}}} + R_BT\left(\lambda - \lambda_*\right). & \text{si } \lambda \geq \lambda_*, \end{cases} \tag{36}$$

We can see that there is actually stress relaxation during the phase transformation, as the factor preceding λ is smaller than 1. Also, as $P_1\left(\lambda_A, 0, T\right) > P_1\left(\lambda_E, 0, T\right)$ relaxation is necessarily larger during crystallization than during fusion. We can see that the model reproduces the main features of the experimental data (figure 7). Finally, on this cycle, the dissipation is

$$D_{cycle} = \frac{\lambda_{\chi,sat}}{2}\left(P_1\left(\lambda_A, 0, T\right) - P_1\left(\lambda_E, 0, T\right)\right). \tag{37}$$

So we have obtained a qualitative modeling of the strain-induced crystallization.

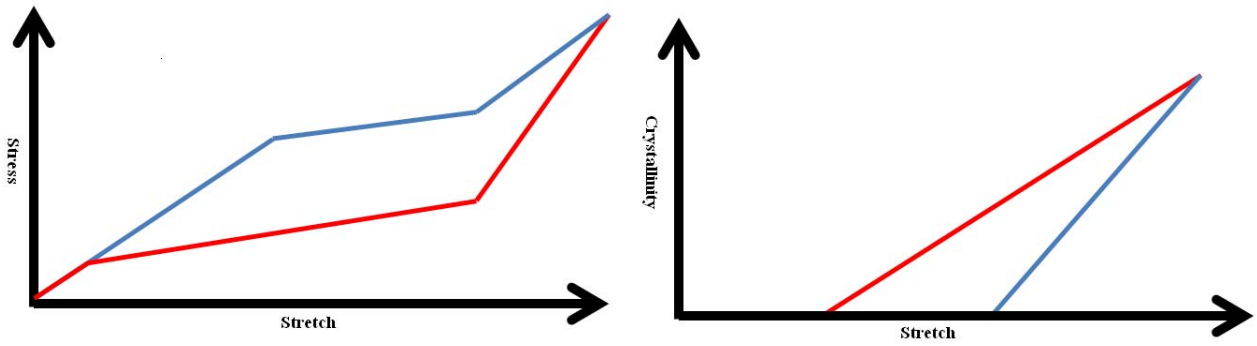

Figure 7: Analytical model (Loading in blue) (Unloading in Red)

5 Numerical testing : Experiment vs Model

In our case, these experiments have been performed with a sample of 1.2g NR at a tensile rate of 2 mm/min submitted to a uniaxial loading-unloading cycle. And, the computed stress is the nominal stress for an uniaxial incompressible elongation.

The figure 8 shows the result of an experiment conducted in order to mimick the behaviour of the pure amorphous part of the material, that is, of the amorphous matrix without crystallization. In order to realize this, the sample is heated at 80 celsius degrees where crystallization does not take place and the curve is transformed by homothetia into an amorphous curve at 40 celsius degrees. The curve obtained through pure modelling is found by using 4 and fitting the constants by a least square method to the experimental curve. The two curves appear to be very similar.

The figure 9 displays the relationship between stress and strain on the same sample quenched at 40. A good agreement between experiment and theory is found if we use power function for the phenomenological terms. In order to obtain the constants of the model, one proceeds by using the phase diagram to get the onset of crystallization and end of fusion, then using the unloading part which is the equilibrium curve. Finally, we optimize the result by looking at F. We have found that all the difficulty is concentrated in the optimization of g. So, we think that the interaction energy should be studied more deeply in its relation to crystal morphologies.

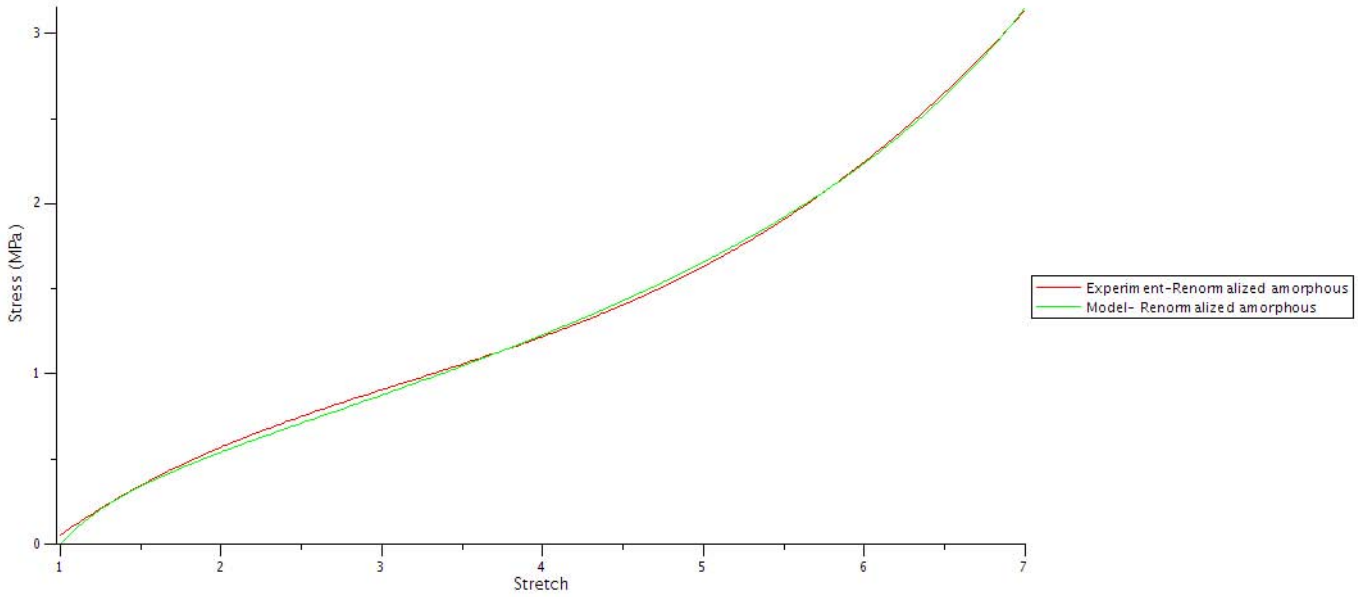

Figure 8: Cyclic loading amorphous

The figure 10 displays the computed λ_χ, the efficient component of crystallinity. This appears to have a behaviour qualitatively similar to the crystallinity curve (figure 11). This may validate an assumption such as we can find a simple function Λ_χ which verified

$$\frac{\mathrm{d}\lambda_\chi}{\mathrm{d}t} = \Lambda(\lambda_\chi)\frac{\mathrm{d}\chi}{\mathrm{d}t}. \tag{38}$$

Such a relationship supposes that once created, a crystallite keeps its morphology. There are three points around which there is discrepancy in the figure 11. The discrepancy around $\lambda = 3$ is due to the error between experiment and model amorphous curves at the end of fusion. The hump juste after unloading can be attributed to the effect of loading rate, which has been taken into account in further work. Finally the incipient cristallinity found at the beginning of crystallization has never been unveiled in stress-strain measurements as it should have if relaxation had occurred. This discrepancy can be attributed to intramolecular crystallization but remain not very clear.

6 Conclusion

In this paper, we have approached the behaviour of natural rubber under stress as simply as possible. For this, a review of existing experiments on the cyclic mechanical behaviour has been done. This literature is quite rich as it displays simultaneous stress-strain and cristallinity measurements.The main features of these curves can therefore be identified, in the sense that the mechanical behaviour between special points of these curves can be linked with microstructural evolution of the semicristalline material. The shape of the curves can be qualitatively explained in terms of micromechanisms.

One then has to set up a proper free energy to describe the system. Prior work by Flory [ref] strongly suggests that there is a contribution of the crystalline part, in terms of elongation, to the amorphous part of the rubber. Therefore the internal variable λ_χ has been considered:, whereλ_χ is the inelastic part of elongation induced by crystallization. Also, hardening of the material linked to microstructural changes has been taken into account by introduction of a

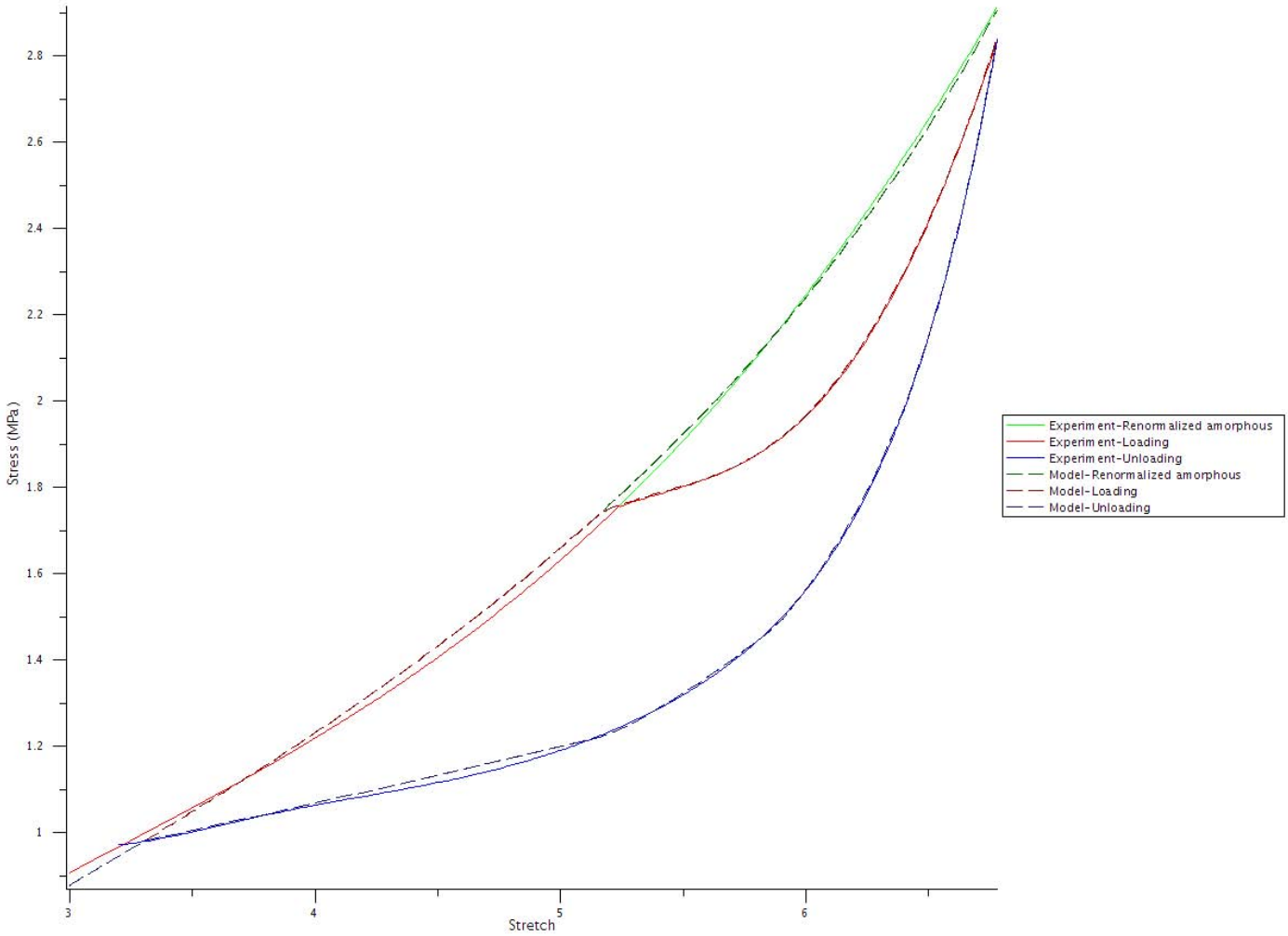

Figure 9: Cyclic loading Stress-Stretch

phenomenological stored energy function of λ_χ.The free energy has then be expressed as a sum of contributions, from the amorphous part, from the matrix-crystallites interaction, and from the crystallites only. Constitutive equations have then been deduced from the second law of thermodynamics. Dissipation is a function of λ, $\lambda_\chi$and T, and the thermodynamical force π_{λ_χ} , a necessary dual variable of $\lambda_\chi$has been introduced. Finally evolution laws have been determined. $\pi_{\lambda_\chi}$was taken to vary between 0 and a critical value describing the delay from equilibrium in terms of λ_χ . We have tested this model with a simplified gaussian model for one chain and a simplified stored energy. The shape of the curves obtained in this way appears to be satisfactory. This is a first step in numerical testing of the model. In addition, this 1D calculation can be associated to a 3D model, and used , as presented in [JG paper], in association with fracture calculations.

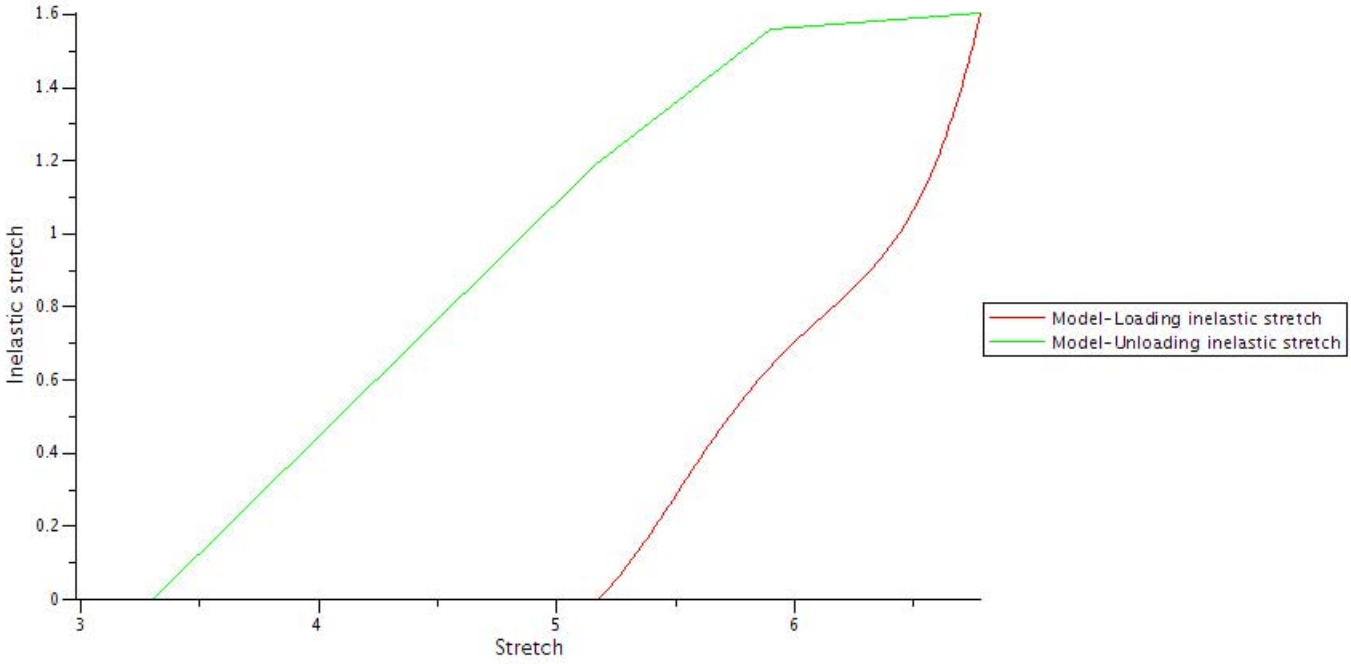

Figure 10: Cyclic loading Inelastic stretch-strech

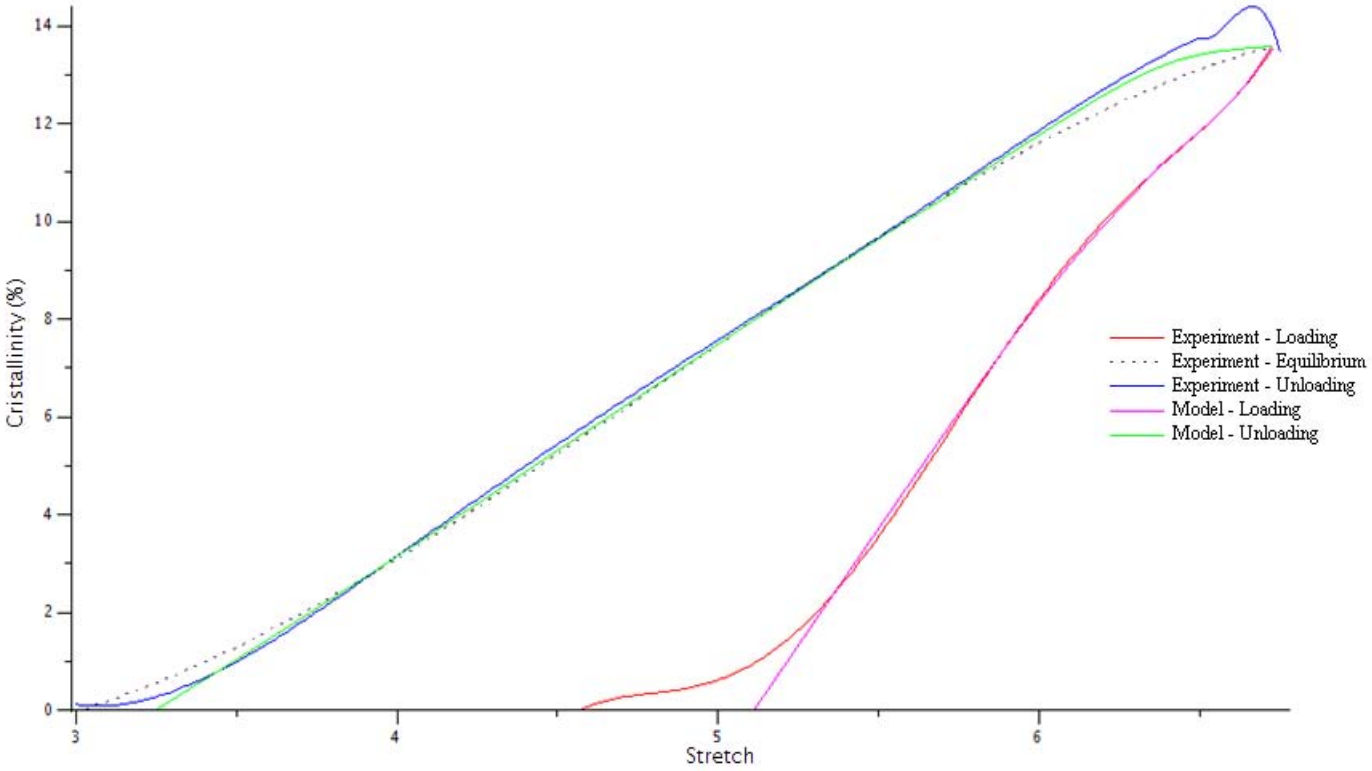

Figure 11: Cyclic loading Crystallinity

REFERENCES

[1] R. Dargazany, M. Itskov: A network evolution model for the anisotropic Mullins effect in carbon black filled rubbers. *International Journal of Solids and Structures*, 46(2009), 2967-2977.

[2] B.Huneau: Strain-induced crystallization of natural rubber: a review of x-ray diffraction investigations. *Rubber chemistry and technology*, 84(2011), 425-452.

[3] J. Marchal: Crystallisation of rubbers filled and unfilled under strain : Effect on the amorphous chains. *Universit Paris Sud - Paris XI (21/06/2006), Jacques Rault (Dir.)*.

[4] Y. Merckel, M. Brieu, J. Diani, J. Caillard: A Mullins softening criterion for general loading conditions. *Journal of the Mechanics and Physics of Solids*, 60(2012), 1257-1264.

[5] C. Miehe, S. Gktepe, F. Lulei: A micro-macro approach to rubber-like materialsPart I: the non-affinemicro-sphere model of rubber elasticity. *Journal of the Mechanics and Physics of Solids*, 52(2004), 2617-2660.

[6] E.A. Poshtan, R. Dargazany, M. Itskov: Modeling of strain-induced crystallization in natural rubbers. *PAMM*, 11(2011), 423-424.

[7] J. Rault, J. Marchal, P. Judeinstein, P. A. Albouy: Chain orientation in natural rubber, Part II: 2H-NMR study. *The european physical journal e: soft matter and biological physics*, 21(2006), 243-261.

[8] N. Saintier, G. Cailletaud, R. Piques: Cyclic loadings and crystallization of natural rubber: An explanation of fatigue crack propagation reinforcement under a positive loading ratio. *Materials Science and Engineering: A*, 528(2011), 1078-1086.

[9] M. Tosaka: A Route for the Thermodynamic Description of Strain-Induced Crystallization in Sulfur-Cured Natural Rubber. *Macromolecules*, 42(2009), 6166-6174.

[10] M. Tosaka, S. Murakami, S. Poompradub, S. Kohjiya: Orientation and Crystallization of Natural Rubber Network As Revealed by WAXD Using Synchrotron Radiation. *Macromolecules*, 37(2004), 3299-3309.

[11] M. Tosaka, K. Senoob, K. Satob, M. Nodab, N. Ohtac: Detection of fast and slow crystallization processes in instantaneously-strained samples of cis-1,4-polyisoprene. *Polymer*, 53(2012), 864-872.